High-Speed Broadband Quantum Efficiency Determination of Solar Cells

Thomas Missbach, Reinhold S. L. Straub, Tobias M. Benkhoff, and Gerald Siefer

***Abstract*—The investigation of the external quantum efficiency (EQE) of optical sensors and solar cells plays a major role in device characterization. As a key parameter, the EQE reveals important information about optical and electrical properties. In the field of photovoltaics, the EQE is, moreover, mandatory for the spectral mismatch correction in the process of device calibration. The work presented here aims for a new measurement method accelerating the time-consuming EQE determination procedure by more than two orders of magnitude. The new set-up is based on a spectrograph system with an integrated spatial light modulator operated as fast amplitude modulating element. This allows utilizing the multiplex advantage by characterizing the sensitivity of the device at various wavelengths at once. An enhanced system is presented, which covers the broadband wavelength range from 300 up to 2000 nm. Thus, it is now possible to determine the EQE of, e.g., germanium-based detectors with an accuracy comparable to standard EQE systems within a few seconds only.**

***Index Terms*—Frequency division multiplex, micromirror device, photovoltaic cell characterization, quantum efficiency measurement, real-time quantum efficiency, spectral responsivity, III–V semiconductors.**

I. Introduction

THE external quantum efficiency (EQE) or spectral responsivity contains exceptional information about the optical and electrical properties of a light-sensitive semiconductor device. With regard to photovoltaics, the EQE measurement is mandatory to apply the spectral mismatch correction in order to determine the efficiency of a solar cell [1]–[3]. To extract this information, the device under test (DUT) is typically operated under short-circuit conditions and illuminated with quasi-monochromatic light. The relation of the current generated by the monochromatically illuminated DUT to the intensity of the light allows determining the EQE. In order to operate the DUT under realistic conditions, an additional continuous background illumination, referred to as bias light, is used during the measurement. By ac-modulating the quasi-monochromatic light, both current components (here the dc component corresponds to the bias illumination and the ac component corresponds to the quasi-monochromatic light) generated in the DUT can be distinguished. This procedure is known as a differential spectral responsivity method [4]. State-of-the-art quantum efficiency measurement systems typically perform the entire EQE measurement sequentially for each single wavelength subinterval within a predefined spectral interval [3]. Consequently, the total measurement time is directly related to the intended optical resolution and bandwidth which in most cases leads to a considerably time consuming process. To overcome this weakness, several multiplex approaches have been published in the past, which improve speed by testing the sensitivity of the DUT at more than one wavelength component at the same time. Typically, these technologies utilize controllable narrowband light sources such as LEDs as presented for instance in [5]–[9]. The time advantage, however, is often paired with a loss of flexibility, bandwidth, and optical resolution. One option to circumvent these drawbacks is the use of a spatial light modulator integrated into a customized spectrograph set-up. The basic concept, first investigations of such a system as well as a comparison of figures of merit with recent high-speed quantum efficiency measurement approaches have been presented in [10] and [11]. The method and system presented here supplement this existing EQE measurement approach. Former bandwidth and accuracy limitations are largely improved by means of an advanced optical system and digital signal processing. Eventually, comprehensive repeatability measurements were carried out in order to validate measurement accuracy.

II. EQE Measurement System Set-Up

The core element of the EQE measurement set-up is a Texas Instruments DLP Technology based spatial light modulator (digital micromirror device) [12] used for frequency division multiplexing (FDM). This allows characterizing the DUT's EQE for multiple quasi-monochromatic wavelengths simultaneously. Fig. 1 illustrates the functional principle. The optical configuration of a diffraction grating (G1) based Czerny–Turner spectrograph enables the isolation of the spectral components generated by the continuous spectrum of, e.g., a short-arc light source [13]. Each wavelength component is then modulated by the spatial light modulator in intensity with a certain frequency and, eventually, recombined to a polychromatic light ray bundle using a second diffraction grating (G2) which is guided onto the DUT

Manuscript received April 5, 2017; revised June 26, 2017; accepted July 18, 2017. Date of publication August 4, 2017; date of current version August 18, 2017. This work was supported by the Federal Ministry for Economic Affairs and Energy (BMWi) under the HeKMod4 project, contract number 0325750. The work of T. Missbach was supported by the fellowship from the Karlsruhe School of Optics & Photonics. *(Corresponding author: Thomas Missbach.)*

T. Missbach and G. Siefer are with the Fraunhofer Institute for Solar Energy Systems ISE, Freiburg 79110, Germany (e-mail: thomas.missbach@ise.fraunhofer.de; gerald.siefer@ise.fraunhofer.de).

R. S. L. Straub was with the Fraunhofer Institute for Solar Energy Systems ISE, 79110 Freiburg, Germany (e-mail: reinhold.straub@koenigsflieger.de).

T. M. Benkhoff was with the Fraunhofer Institute for Solar Energy Systems ISE, 79110 Freiburg, Germany (e-mail: tobias@benkhoff.com).

Color versions of one or more of the figures in this paper are available online at http://ieeexplore.ieee.org.

Digital Object Identifier 10.1109/JPHOTOV.2017.2730885

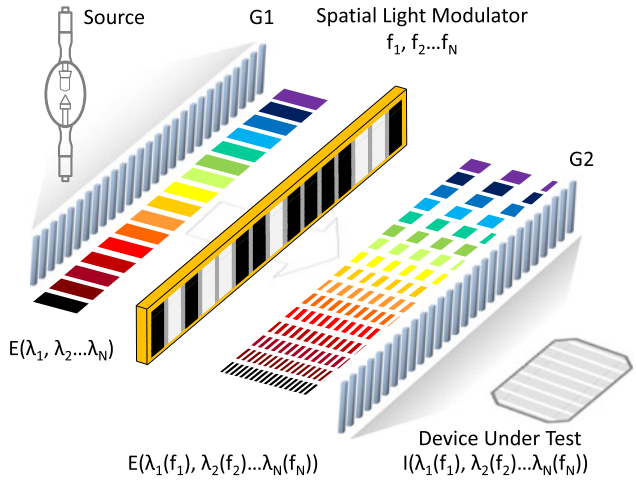

Fig. 1. Schematic diagram of the spatial light modulator based measurement setup. By a first diffraction, grating G1 polychromatic light from a short-arc source is fanned out into its quasi-monochromatic components. Once these components were amplitude modulated utilizing a spatial light modulator, a second diffraction grating G2 is used to recombine the monochromatic components. Illustration derived from [11].

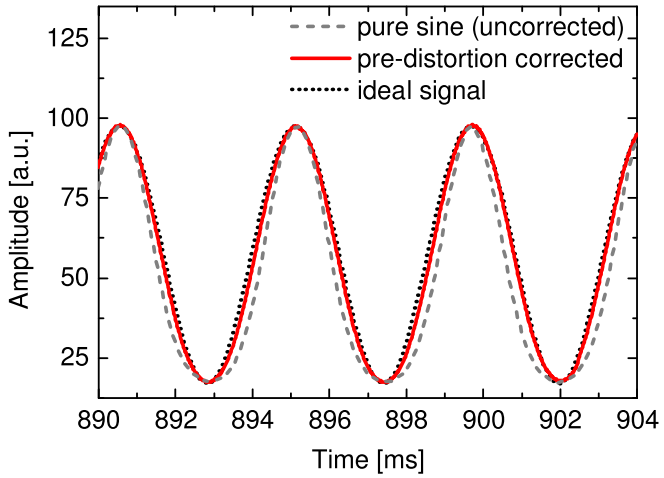

Fig. 2. Detail of a single sinusoid received by a 4 cm^2 Ge solar cell at 532 nm amplitude modulated with 409.5 Hz. The dashed line shows the modulation with a single-term sinusoidal modulation pattern. The solid line shows the improved version using the first and second term of a Fourier series in order to compensate for illumination inhomogeneity. For reference, an ideal sinusoidal signal is shown by the dotted curve.

[11]. Finally, the current signal generated by the illuminated DUT can be decoded by analyzing the Fourier components of its current spectrum. Thus, the possible time improvement of this approach is proportional to the number of time-parallel measurements, respectively, spectral components.

In practice, however, the absence of slow rotating mirrors or diffraction gratings for wavelength selection used in conventional monochromators as well as noise relevant improvements of the signal processing chain allows for even higher speed improvements without compromising accuracy significantly.

A. Signal Generation and Processing

Pattern generation plays a major role in high accuracy signal processing by means of light modulating elements. The high pixel density of the used light modulator of 1024 × 768 micromirrors [12] allows on one hand for reasonable optical resolutions [11], [10] but it also enables varying the amplitude with an accuracy of more than 9-bit resolution. This opens up the possibility of modulating more noise robust sinusoidal signals instead of simple rectangular ON–OFF switching patterns [11]. However, the use of a high power arc lamp directly illuminating the spectrograph set-up comes at the cost of illumination homogeneity. The spectral focal plane of the light modulator shows, therefore, an in homogeneous Gaussian-shaped light intensity distribution according to the distribution in the entrance slit plane of the first spectrograph stage (represented by G1 in Fig. 1). If the sinusoidal bit pattern or rather the micromirror assignment is performed under the assumption of perfect homogeneous illumination, inhomogeneity in the space domain will lead to distortion in the time domain of the resulting sinusoidal waveforms. If one considers purely time domain behavior, the inhomogeneity influence can be translated to the time domain by multiplying the modulating function with an angle-dependent amplitude coefficient, whose characteristic is equal to the intensity distribution function in space domain. Thus, the measurement system accuracy will be downgraded due to higher order harmonics.

A simple and effective strategy to improve precision is to predistort the sinusoidal signal generation in order to compensate for the spatial illumination inhomogeneity. The non-predistorted modulation function used by default is given by

$$A_{\text{pattern}}(t) = \sin\left(2\pi \frac{f_{\text{pattern}}}{f_s} t + \varphi\right) \tag{1}$$

and can be substituted by a Fourier series according to

$$A_{\text{pattern}}(t) = \sum_{n=1}^{N} \left(a_n \sin\left(2\pi \frac{f_{\text{pattern}}}{f_s} t + n\varphi\right)\right). \tag{2}$$

In both cases, the parameters f_{pattern} and f_s represent the appropriate modulation frequency and sampling frequency.

Fig. 2 shows the results of a single sinusoidal signal measured by a 4 cm^2 Germanium solar cell at 532 nm modulated with 409.5 Hz with and without predistortion/correction. For comparison, also the simulated ideal signal curve, represented by the dotted line, is shown. The frequency and phase parameters used for the Fourier series correction procedure were determined from the sinusoidal modulation measurement without predistortion/correction utilizing fast Fourier transformation. Phase parameters were located using the cross correlation method. The resulting total harmonic distortion (THD) is without correction (dashed line in Fig. 2) dominated by the first harmonic and greater than 19.6%. By using predistorted modulation patterns with as few as $N = 2$ terms (solid line in Fig. 2), the THD can already be decreased to values below 1.25%. A useful additional side effect is the reduction of overlaps between higher modulation frequencies and harmonics of lower modulation frequencies.

The modulation pattern configuration is, in general, equal to a frequency comb f_{comb} with the frequency domain

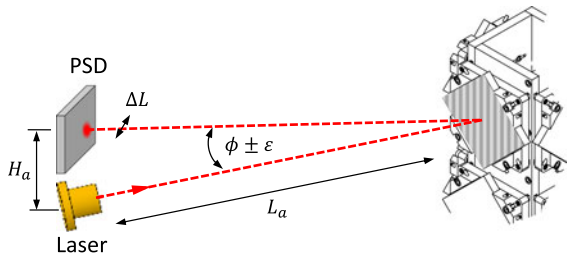

Fig. 3. Sketch of the triangulation measuring arrangement used for the angular accuracy characterization. The position of the laser spot was measured by a due-lateral position sensitive device (PSD).

representation according to

$$f_{\text{comb}} = f_0 + \sum_{n=0}^{N} n \cdot f_d. \tag{3}$$

For all results presented here, f_0 was set to 314.6 Hz and f_d to 8.33 Hz. This frequency scheme was chosen in order to avoid overlaps with harmonics and integral multiples of 50 Hz (Germany mains frequency).

B. Optical System

Compared to [11], the enhanced measurement set-up presented here covers a significantly larger wavelength range. This is accomplished by utilizing four sets of different diffraction gratings with diverse efficiency regions matched to the respective wavelength interval. For automation, the gratings were mounted on a fast rotational stage (OWIS GmbH DMT 100-D53-HiDS).

In relation to the rotational stage axis, each grating is aligned diagonally originating from the idiosyncratic orientation of the micromirrors of the used spatial light modulator [12]. Therefore, the positioning accuracy of the rotating stage has an immediate effect on both, wavelength accuracy and angular beam scattering. The low groove densities of the diffraction gratings used in this application lead to a large reciprocal angular dispersion of up to 166 nm/°, thus demanding high angular positioning accuracy. In order to characterize and calibrate the rotational stage, the triangulation method was used. Fig. 3 shows a sketch of the applied set-up. The grating rotational stage was equipped with a standard broadband mirror reflecting the ray of a 685 nm diode laser to the surface of a duo-lateral position sensitive device (PSD) [14], [15]. The accuracy examination was repeated for 250-times at different turning speeds from 40 up to 80°/s.

The laser spot position on the PSD was obtained by the intensity corrected position according to (4). The currents I_a and I_b represent the PSD electrode currents related to the horizontal plane:

$$\Delta L = L \cdot \frac{I_a - I_b}{2 \cdot (I_a + I_b)}. \tag{4}$$

The position error ΔL was mean corrected to ΔL_{rel} and eventually used to calculate the angular position error:

$$\varepsilon = \sin^{-1}\left(\frac{H_a}{L_a} + \Delta L_{\text{rel}}\right) - \frac{\Phi}{2}. \tag{5}$$

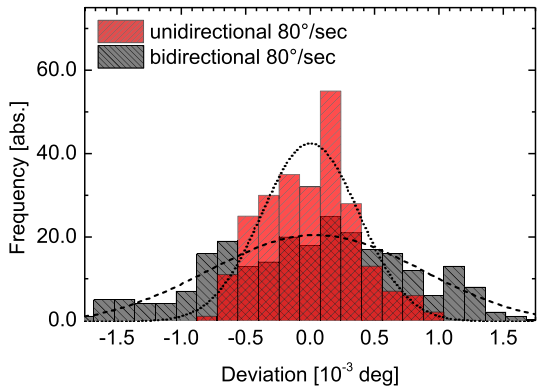

Fig. 4. Angular error distribution of 250 repeat measurements in unidirectional and bidirectional movement modes at the highest speed of rotation. The dashed and dotted curves indicate the Gauss fit to the histograms.

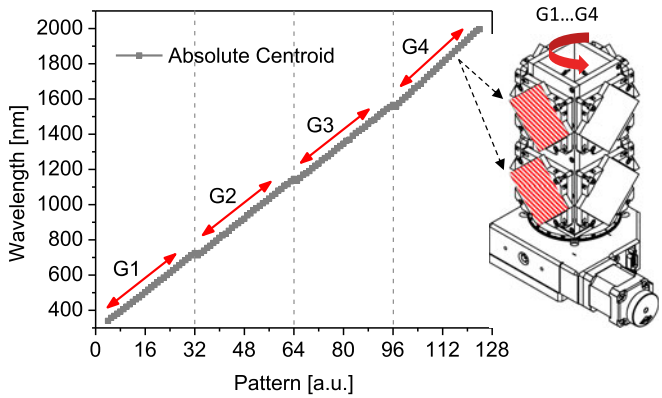

Fig. 5. Linearity measurement of the improved setup equipped with all four sets of gratings. Micromirrors were sequentially pattern-wise activated and have been investigated in respect to their spectral centroids for each diffraction grating set.

Using a 16 mm^2 PSD ($L = 4$ mm) in a spectrograph optical setup with 300 mm focal length (equal to L_a and $H_a = 65$ mm) yielded to the angular error distributions as shown in Fig. 4. Both measurements were performed at the highest rotational speed of 80°/s in unidirectional and bidirectional mode. The standard deviation of the fitted Gauss curves (dashed and dotted lines) is 0.0084° (bidirectional) and 0.0038° (unidirectional). This corresponds to deviations in wavelength of 1.4 and 0.6 nm, respectively. Thus, it is worthwhile to operate the rotational stage in unidirectional mode at the cost of flexibility and speed. The reduction of the rotational speed to 60 or 40°/s showed a negligible effect on positioning accuracy. It is, additionally, important to mention that the measurement error of the electro optical measuring arrangement was dominated by the PSD and is in the order of ±0.1 nm [15].

Another important factor concerning measurement accuracy is the linearity of single quasi-monochromatic components. In [10], a linearity evaluation was already performed for a single diffraction grating-set by evaluating the centroid of the dispersed spectrum selected by sequentially pattern-wise activated micromirrors. To complement this, Fig. 5 shows the measurement results of the improved setup equipped with all four sets of gratings.

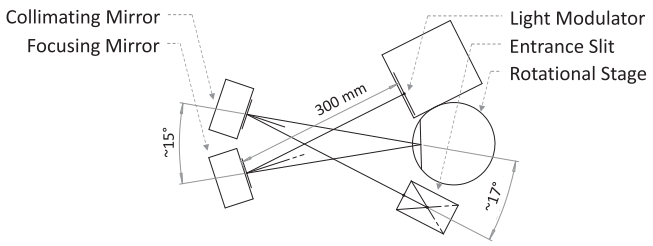

Fig. 6. Sketch of the arrangement of optical components for a single diffraction grating stage. Crossing of the optical path allowed it to greatly reduce aberrations due to off-axis illumination of spherical optical elements.

TABLE I
WAVELENGTH CONFIGURATION OF THE EQE SPECTROGRAPH

Grating set	Interval calculated [nm]	Interval measured [nm]	Spectral bandwidth (deviation) [nm]
1	300.0–729.0	298.0–730.0	432.1 (+3.0)
2	719.0–1147.6	717.1–1151.4	434.3 (+5.7)
3	1137.6–1565.7	1140.6–1575.0	434.4 (+6.3)
4	1555.7–2059.1	1566.0–2076.2	510.3 (+6.9)

Overview of the diffraction grating configuration used in the new broadband quantum efficiency measurement system. Grating sets 1–3 are 100 grooves/mm types. For the sake of efficiency diffraction grating set 4 features 80 grooves/mm. This leads to a slightly broader optical bandwidth and, in turn, marginal reduced optical resolution. Calculated values result from the paraxial approximation and show a good agreement with the respective measurement values.

In order to cover the entire wavelength range of the optical system, an advanced rack-mount spectrometer system consisting of three dedicated diode array spectrometers (Carl Zeiss MMS1 NIR enhanced, PGS NIR 1.7-256, PGS NIR 2.0-256) was used. Ideally, all centroid wavelength values should form a perfect linear slope, only disrupted by small overlaps between the dispersion of consecutive gratings. These dispersion sections are segmented and highlighted by the vertical dashed lines in Fig. 5. By means of regression analysis, the total standard deviation of all four sections was examined to be below 0.17%. Compared to [10] and [11], this indicates an improvement of almost 40%. The main reasons for this are reduced optical aberrations due to an improved crossed Czerny–Turner spectrograph layout, as shown (for a single diffraction grating stage) by Fig. 6. This allowed decreasing the diffraction grating inclusion angle, formed by the intersection of the central light rays in the grating plane, from 19° to 15°. In this way, optical aberrations have been greatly reduced.

Table I shows the calculated and measured wavelength intervals per grating set. Calculated values result from the paraxial approximation. For the grating sets 1–3, which cover the spectral range from about 300 to 1600 nm, 100 grooves/mm grating types were used. For the sake of efficiency and availability, diffraction grating set 4, however, features 80 grooves/mm. This leads to a slightly broader optical bandwidth and, in turn, marginal reduced optical resolution for the spectral interval ranging from about 1600 to 2100 nm. The small difference between calculated and measured spectral bandwidth (right column—deviation) originates mostly from adjustment imperfections and optical

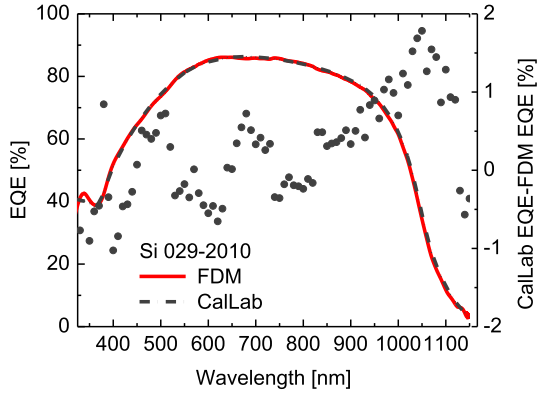

Fig. 7. Comparison of measurement results of the same silicon solar cell using Fraunhofer ISE calibration lab test equipment (CalLab, dash-dotted line) and the new modulating EQE measurement system (FDM, solid line). The absolute difference is represented by the solid dots and the right *y*-axis.

aberrations caused by off-axis illumination of focusing and collimating (spherical) mirrors.

For the subsequent measurements, the spatial light modulator was sectioned into 64 equally spaced modulating patterns. With respect to optical resolution, full-width at half-maximum values of 7–8 nm for quasi-monochromatic components isolated by diffraction grating-sets 1–3 and around 8–9 nm using grating-set 4 were characterized by spectrometer measurement series.

III. QUANTUM EFFICIENCY MEASUREMENTS

To guarantee comparability, all further investigations have been carried out using a set of calibrated silicon and germanium solar cells for both, the new measurement setup presented here as well as the reference laboratory system at ISE CalLab (the solar cell calibration laboratory at Fraunhofer ISE) [1]. In order to determine the EQE of the respective test cell, the measured current was weighted with the transfer function which has been computed from the calibrated EQE and the current response of the reference cell. The impact of inhomogeneity of the measurement light spot is considered to be negligible as the illuminated area was chosen smaller than the active area of the cell under measurement. Regarding the electronic signal acquisition, a customized composite wideband transimpedance amplifier was developed for the new setup. It is based on a linear technology LT6018 integrated operational amplifier [16] buffered by an additional dc stabilized low noise input stage. By utilizing a current booster circuitry, the amplifier covers the relevant frequency range from dc to 5 kHz at input currents from 5 pA up to 1 A. The resulting analog voltage signal is then quantized with 100 kSPS using a 24-bit data acquisition system (m + p VibPilot). The entire measurement set-up is synchronized with the spatial light modulator as well as the rotational grating stage and fully automated via C++ and LabView software.

A. Quantum Efficiency Measurements

Fig. 7 shows the comparison of two measurements of the identical 4 cm^2 silicon solar cell (id: 029-2010) performed using the conventional ISE CalLab grating monochromator-based system

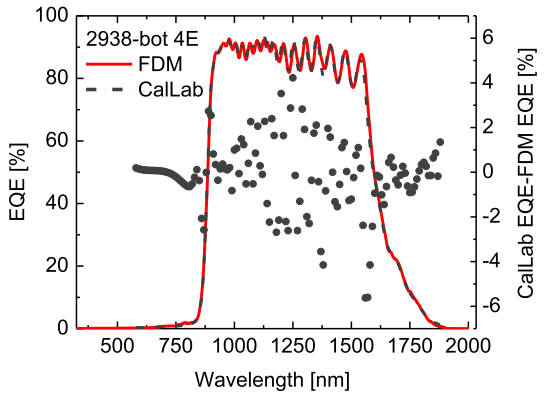

Fig. 8. Comparison of the measurements of a 4 cm^2 Germanium component/isotype cell. The solid curve represents the measurement results using the new high-speed setup. The dash-dotted line corresponds to the reference measurement. The absolute difference between both measurements is given by solid dots and the right-hand side *y*-axis.

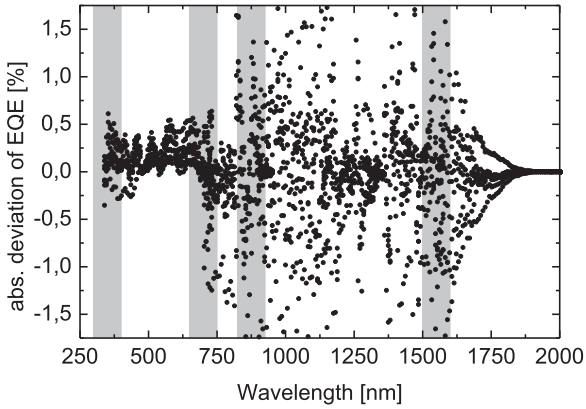

Fig. 9. Results of the reproducibility measurement campaign. The dots represent the difference of the first to every other measurement of a test series. Regions of steep variation of the spectral response of the used solar cells are highlighted by grey bars. The largest variations in the wavelength interval from 900 to 1600 nm are subject to reduced light intensity as well as small wavelength scale mismatch introduced by mechanical variation of the grating rotational stage in combination with the oscillations in the Ge EQE.

(CalLab—dash-dotted line) and the new high-speed measurement system (FDM—solid line).

The conventional measurement took around 30 min, while the modulated FDM measurement was completed after 23 s. The measurement of the interval of spectral components dispersed by a single diffraction grating, however, took solely 1.8 s. Therefore, the vast majority of the measurement time was consumed by the rotating stage still indicating room for improvements. It should be noted that 23 s cover already the full wavelength range from 298 up to 2076.2 nm including all four diffraction grating sets. The absolute deviation between the FDM measurement and the (interpolated) ISE CalLab reference is represented by the solid dots and the right *y*-axis. The deviation increases from below $\pm 1\%$ for wavelengths lower than 1000 nm slightly up to $\pm 2\%$ for steeper regions of the EQE curve toward the silicon band edge. This effect is mainly attributed to a small wavelength shift which originates from wavelength calibration inaccuracy. The full-scale standard deviation amounts, therefore, 0.71% (EQE, absolute).

In order to examine the accuracy of the new system at higher wavelengths above 1100 nm, a 4 cm^2 single-junction germanium cell (bottom component/isotype of a triple-junction solar cell with electrically inactive top and middle cell) was chosen [17]. Due to interference effects at the thin semiconductor layers on top of the active germanium cell that are intended to simulate the absorption situation in the corresponding multijunction device, the EQE curve of this cell exhibits detailed oscillations. The graph in Fig. 8 again shows a comparison of the EQE characterized with the conventional Fraunhofer ISE CalLab equipment as well as utilizing the new high-speed set-up. Here, the total time of the measurement performed in conventional fashion amounted nearly 60 min in contrast to the modulated measurement with 23 s. The curve oscillations greatly reveal the wavelength scale mismatch also observed in Fig. 7, which causes larger EQE deviations of up to +4/–5.9% (represented by the dots). The standard deviation is in the range of 1.91% (EQE, absolute). In general, however, the optical resolution of the new set-up is sufficient to fully resolve the oscillations and their almost exact positions, corresponding to the CalLab reference measurement.

B. Reproducibility

In order to gain a realistic evaluation of the reproducibility of EQE measurements utilizing the new set-up, a series of repeat measurements has been carried out. To cover the (almost) entire available wavelength range, three different 4 cm^2 single-junction component/isotype solar cells ($Ga_{0.50}In_{0.50}P$, $Ga_{0.99}In_{0.01}As$, Ge) were used. For each cell, the EQE was measured 20 times consecutively. Eventually, the deviation of the first to every other measurement of each test series was computed. Fig. 9 shows the results of all three test series consisting of 60 combined EQE measurements. The cumulative standard deviation amounts to 0.52%. Transition regions in the EQE curves of the used solar cells are highlighted by grey bars. Especially steep variations in the spectral response curves as well as the modulating response of the used bottom isotype solar cell above 900 nm (shown in Fig. 8) affect repeatability. Here, moreover, the wavelength shift introduced by the grating rotational stage, observed in Fig. 4, comes into play. For example, a wavelength shift of ± 1 nm at 1250 nm can cause $\pm 3.6\%$ EQE variation.

Further accuracy degrading influence is assigned to the reduced infrared light intensity of the short-arc xenon source. It has to be noted that the intensity variation of the light source was not actively monitored during measurement. The implementation of a monitoring device is already foreseen and is expected to further improve measurement accuracy. The region above 1800 nm of Fig. 9 exhibits approximately zero variations due to the spectral response (see Fig. 8) of the germanium subcell, which slopes toward zero.

IV. Conclusion

A new high-speed EQE measurement set-up was presented which overcomes bandwidth limitations of former high-speed systems while maintaining a high degree of measurement accuracy. Sample measurements on silicon- and germanium-based

solar cells demonstrated that the new set-up covers the spectral interval ranging from 300 up to 2000 nm. Accuracy was investigated by comparative measurements with Fraunhofer ISE CalLab EQE calibration equipment. Despite the early development stage of our new system, the measurement standard deviation is already in the range of 1.9% EQE over full bandwidth. Repeatability measurements showed standard deviations in the range of 0.5% EQE. The obtained measurement time reduction is in the order of 100-times and more compared to state-of-the-art measurement technology. Thus, EQE characterization can be performed within seconds instead of hours. This opens up new fields of applications such as inline measurements, spatial resolved measurements, or characterization under varying bias light conditions.

Our future research activities in this field aim toward a measurement system capable also for the fully automated measurement of multijunction solar cells. For this purpose, a spatial light modulator based arbitrary tunable bias light source is under development. Another research focus is the more detailed analysis of measurement accuracy supplemented by improvements on signal processing with regard to precision and reliability.

ACKNOWLEDGMENT

The authors are responsible for the content of this paper. They gratefully acknowledge rotational stage characterization measurements by J. Xu as well as solar cell calibration measurements by M. Schachtner conducted at the Fraunhofer ISE CalLab.

REFERENCES

[1] C. H. Seaman, "Calibration of solar cells by the reference cell method - The spectral mismatch problem," *Sol. Energy*, vol. 29, no. 4, pp. 291–298, 1982.

[2] "Photovoltaic devices Part 7: Computation of the spectral mismatch correction for measurements of photovoltaic devices," IEC Std. 60904-7 Ed. 2.0, 2007.

[3] G. Siefer, T. Gandy, M. Schachtner, A. Wekkeli, and A. W. Bett, "Improved grating monochromator set-up for EQE measurements of multi-junction solar cells," in *Proc. 39th IEEE Photovolt. Spec. Conf.*, Tampa, FL, USA, 2013, pp. 86–89.

[4] J. Metzdorf, "Calibration of solar cells. 1. The differential spectral responsivity method," *Appl. Opt.*, vol. 26, pp. 1701–1709, 1987.

[5] D. L. Young, B. Egaas, S. Pinegar, and P. Stradins, "A new real-time quantum efficiency measurement system," in *Proc. 33rd IEEE Photovolt. Spec. Conf.*, San Diego, CA, USA, 2008, pp. 1–3.

[6] J. Schmidt *et al.*, "Characterization and gauge study of a high speed quantum efficiency apparatus," in *Proc. 35th IEEE Photovolt. Spec. Conf.*, 2010, pp. 1710–1714.

[7] W. Reetz *et al.*, "A novel high speed spectral response measurement system based on LED light sources," in *Proc. 26th Eur. Photovolt. Sol. Energy Conf. Exhib.*, 2011, pp. 113–116.

[8] B. H. Hamadani, J. Roller, B. Dougherty, and H. W. Yoon, "A versatile light-emitting-diode-based spectral response measurement system for photovoltaic device characterization," *Appl. Opt.*, vol. 51, pp. 4469–4476, 2012.

[9] J. A. Rodriguez, M. Vetter, M. Fortes, and C. Alberte, "Development of a very fast spectral response measurement system for silicon thin film modules," in *Proc. 2013 Spanish Conf. Electron Devices*, 2013, pp. 369–372.

[10] T. Missbach, C. Karcher, G. Siefer, and A. W. Bett, "Frequency division multiplex-based light spectroscopy," *Opt. Soc. Amer., Opt. Express*, vol. 23, no. 19, pp. 24634–24647, 2015.

[11] T. Missbach, C. Karcher, and G. Siefer, "Frequency division multiplex based quantum efficiency determination of solar cells," *IEEE J. Photovolt.*, vol. 6, no. 1, pp. 266–271, Jan. 2016.

[12] Texas Instruments Incorporated, "DLP 0.7 XGA 2xLVDS Type A DMD (Rev. B)," Texas Instrum. Inc., Dallas, TX, USA, Rep. no. DLPS026B, Datasheet, 2013. Accessed on: May 27, 2014.

[13] M. Czerny and A. F. Turner, "Über den astigmatismus bei spiegelspektrometern," *Zeitschrift für Physik*, vol. 61, pp. 792–797, 1930.

[14] T. Missbach and J. Jaus, "A new sensor for measuring tracking accuracy, tracker vibration and structural deflection," in *Proc. AIP Conf.*, vol. 1477, pp. 262–266, 2012.

[15] Datasheet DL16-7 First Sensor AG, "DL16-7 SMD," Rev. 04-07-11, Datasheet, 2011. Accessed on: Dec. 22, 2016.

[16] Datasheet LT6018 Linear Technology Corporation, "LT6018, ultralow noise, precision op amp," Rev. 6018f, Datasheet, 2016. Accessed on: Dec. 22, 2016.

[17] J. Jaus, T. Mißbach, S. P. Philipps, G. Siefer, and A. W. Bett, "Spectral measurements using component cells: Examinations on measurement precision," in *Proc. 26th Eur. Photovolt. Sol. Energy Conf. Exhib.*, 2011, pp. 176–181.

Thomas Missbach received the B.Eng. degree in electrical engineering from Koblenz University of Applied Sciences, Koblenz, Germany, in 2011, and the M.S. degree in electrical engineering from the Technical University Munich, Munich, Germany, in 2013. He is currently working toward the Ph.D. degree in electrical engineering focusing on semiconductor measurement technology in cooperation from the Karlsruhe Institute of Technology, Karlsruhe, Germany.

From 2004 to 2013, he was involved in analog hardware design and hardware-related software development in industry. In 2013, he joined the division "Materials - Solar Cells and Technology," Fraunhofer Institute for Solar Energy Systems ISE.

Reinhold S. L. Straub received the B.Eng. degree in mechatronics from Ulm University of Applied Sciences, Ulm, Germany, in 2015.

For attaining the bachelor degree in 2015, he was part of the division "Materials - Solar Cells and Technology," Fraunhofer Institute for Solar Energy Systems ISE, Freiburg, Germany, to support in the fields of system integration and mechanical design.

Tobias M. Benkhoff received the B.Eng. and M.Eng. degrees in electrical engineering/information technology from the University of Applied Sciences and Arts, Göttingen, Germany, in 2013 and 2016, respectively.

The focus of his studies was on signal processing and electronics. At the Fraunhofer Institute for Solar Energy Systems ISE, he was responsible for FPGA-based real-time signal acquisition. Currently, he is involved in electronics and software development for automation of vacuum soldering systems with budatec GmbH, Berlin, Germany.

Gerald Siefer as an Assistant Student in 1977 joined the Fraunhofer Institute for Solar Energy Systems, Freiburg, Germany, where he received the Ph.D. on the topic of "Analysis of the performance of multijunction cells under realistic operating conditions" in 2008.

Since then, his work has been focused on the characterization and calibration of photovoltaic devices. Since 2009, he has been leading the team "III–V cell and module characterization." His team is working on calibration techniques for multijunction solar cells with up to 6 pn junctions for space and terrestrial concentrator applications as well as on the indoor and outdoor characterization of concentrator modules.